Accepted Manuscript

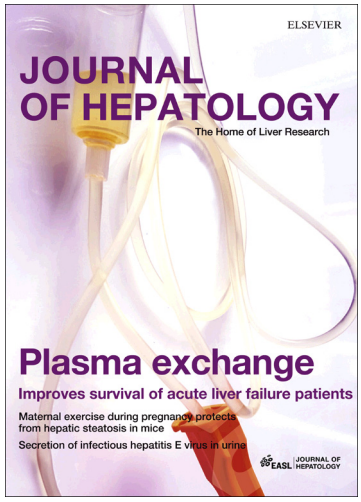

Vps33b is Crucial for Structural and Functional Hepatocyte Polarity

Joanna Hanley, Dipok Kumar Dhar, Francesca Mazzacuva, Rebeca Fiadeiro, Jemima J. Burden, Anne-Marie Lyne, Holly Smith, Anna Straatman-Iwanowska, Blerida Banushi, Alex Virasami, Kevin Mills, Frédéric P. Lemaigre, AS. Knisely, Steven Howe, Neil Sebire, Simon Waddington, Coen C. Paulusma, Peter Clayton, Paul Gissen

PII: S0168-8278(17)30005-3
DOI: http://dx.doi.org/10.1016/j.jhep.2017.01.001
Reference: JHEPAT 6381

To appear in: *Journal of Hepatology*

Received Date: 25 July 2016
Revised Date: 1 December 2016
Accepted Date: 3 January 2017

Please cite this article as: Hanley, J., Kumar Dhar, D., Mazzacuva, F., Fiadeiro, R., Burden, J.J., Lyne, A-M., Smith, H., Straatman-Iwanowska, A., Banushi, B., Virasami, A., Mills, K., Lemaigre, F.P., Knisely, AS., Howe, S., Sebire, N., Waddington, S., Paulusma, C.C., Clayton, P., Gissen, P., *Vps33b* is Crucial for Structural and Functional Hepatocyte Polarity, *Journal of Hepatology* (2017), doi: http://dx.doi.org/10.1016/j.jhep.2017.01.001

Vps33b is Crucial for Structural and Functional Hepatocyte Polarity

Joanna Hanley[1], Dipok Kumar Dhar[2,3], Francesca Mazzacuva[1], Rebeca Fiadeiro[3], Jemima J. Burden[3], Anne-Marie Lyne[4], , Holly Smith[3], Anna Straatman-Iwanowska[3], Blerida Banushi[3], Alex Virasami[5], Kevin Mills[1], Frédéric P. Lemaigre[6], AS Knisely[7], Steven Howe[1], Neil Sebire[5], Simon Waddington[8], Coen C. Paulusma[9], Peter Clayton[1], Paul Gissen[1, 3, 10*].

Author affiliations: [1]UCL Institute of Child Health, University College London, London, WC1N 1EH, UK; [2]Organ transplantation Centre and Comparative Medicine Department, King Faisal Specialist Hospital and Research Centre, Riyadh 11211, Saudi Arabia; [3]MRC Laboratory for Molecular Cell Biology, University College London, London, WC1E 6BT, UK; [4]UCL Department of Statistical Science, University College London, London, WC1E 6BT, UK; [5]Histopathology Department, Camelia Botnar Laboratories, Great Ormond Street Hospital for Children NHS Trust, London, WC1N 3JH, UK; [6] Université Catholique de Louvain, de Duve Institute, 1200 Brussels, Belgium; [7]Institut für Pathologie, Medizinische Universität Graz, 8036 Graz, Austria; [8]UCL Institute for Women's Health, University College London, London, WC1E 6AU, UK; [9]Tytgat Institute for Liver and Intestinal Research, Academic Medical Center, 1105 BK Amsterdam, Netherlands; [10]Inherited Metabolic Disease Unit, Great Ormond Street Hospital for Children NHS Trust, London, WC1N 3JH, UK.

Corresponding author: *Professor Paul Gissen

MRC Laboratory for Molecular Cell Biology, University College London, London, WC1E 6BT, UK

Tel: +44(0)2076793531

Fax: +44(0)2076797805

Email: p.gissen@ucl.ac.uk

Keywords: Vps33b, hepatocyte polarity, canalicular membrane, cholestasis, protein trafficking, Rab11a, gene transfer.

Abbreviations: VPS33B, vacuolar protein sorting 33 homolog; ARC, arthrogryposis renal dysfunction and cholestasis; AAV, adeno-associated virus; HOPS, homotypic fusion and vacuole protein sorting; CORVET, class C core vacuole/endosome tethering; ARE, apical recycling endosome; ALP, alkaline phosphatase; DCA, deoxycholic acid; CDCA, chenodeoxycholic acid; GDCA, glycodeoxycholic acid; GCDCA, glycochenodeoxycholic acid; TDCA, taurodeoxycholic acid; TCDCA, taurochenodeoxycholic acid; taurocholic acid; diOH-C, dihydroxycholanoates; glyco-diOH-C, glycodihydroxycholanoates; tauro-diOH-C, taurodihydroxycholanoates; CLF, cholyl-L-lysyl-fluorescein; MRP2, multidrug resistance-associated protein 2; FD-40, 40KDa fluorescein isothiocyanate conjugated dextran; TEM, transmission electron microscopy; ALT, alanine aminotransferase; IQR, interquartile range; BSEP, bile salt export pump; ABCG8, ATP binding cassette subfamily G member 8; CEA, carcinoembryonic antigen; PLS, partial least squares; DAVID, database for annotation visualisation and integrated discovery; GO, gene ontology; GSEA, gene set enrichment analysis; h*VPS33B*, human *VPS33B* cDNA; h*VPS33B*co, codon optimised human *VPS33B* cDNA; CLDN 1, Claudin1; ANOVA, analysis of variance; PFIC2, progressive familial intrahepatic cholestasis type 2; TGN, trans-golgi network; CA, cholic acid; GCA, glycocholic acid; TCA, taurocholic acid.

Word count: 6979

Figures and tables: 6 figures, 2 tables, 11 supplementary figures, 2 supplementary tables.

Conflict of interest: The authors declare no conflict of interest.

Financial support: Children's Liver Disease Foundation (CLDF), Great Ormond Street Hospital and UCL Institute of Child Health Biomedical Research Centre. P.G. is a Welcome Trust senior clinical research fellow. J.J.B. is supported by core funding to MRC_UCL LMCB university unit (grant ref. MC_U122665002).

Author contribution: J.H. performed experiments, contributed to overall study design and wrote the manuscript which was edited by all co-authors. D.D., F.M., J.J.B., R.F., H.S., A.S-I., B.B., A.V. and S.W. performed experiments. A.M-L. performed *in silico* gene expression and pathway analysis. D.D., J.J.B., K.M., F.P.L., A.S.K., S.H., N.S., S.W., C.C.P., P.C. and P.G. contributed to overall study design. P.G. directed the study.

Abstract (247 words)

Background

In the normal liver, hepatocytes form a uniquely polarised cell layer that enables movement of solutes from sinusoidal blood to canalicular bile. Whilst several cholestatic liver diseases with defects of hepatocyte polarity have been identified, the molecular mechanisms of pathogenesis are not well defined. One example is arthrogryposis, renal dysfunction and cholestasis syndrome, which in most patients is caused by *VPS33B* mutations. VPS33B is a protein involved in membrane trafficking that interacts with RAB11A at recycling endosomes. To understand the

pathways that regulate hepatocyte polarity better, we investigated VPS33B deficiency using a novel mouse model with a liver-specific *Vps33b* deletion.

Methods

To assess functional polarity, plasma and bile samples were collected from *Vps33b* liver knockout (*Vps33b*$^{fl/fl}$*-AlfpCre*) and control (*Vps33b*$^{fl/fl}$) mice; bile components or injected substrates were quantitated by mass spectrometry or fluorometry. For structural analysis, livers underwent light and transmission electron microscopy. Apical membrane and tight junction protein localisation was assessed by immunostaining. Adeno-associated virus vectors were used for *in vivo* gene rescue experiments.

Results

Like patients, *Vps33b*$^{fl/fl}$*-AlfpCre* mice showed mislocalisation of ATP-binding cassette proteins that are specifically trafficked to the apical membrane via Rab11a-positive recycling endosomes. This was associated with retention of bile components in blood. Loss of functional tight junction integrity and depletion of apical microvilli were seen in knockout animals. Gene transfer partially rescued these defects.

Conclusions

Vps33b has a key role in establishing structural and functional aspects of hepatocyte polarity and may be a target for gene replacement therapy.

Lay Summary

Hepatocytes are liver cells with tops and bottoms; that is, they are polarised. At their bottoms they absorb substances from blood. They then, at their tops, secrete these substances and their metabolites into bile. When polarity is lost, this directional flow of substances from blood to bile is disrupted and liver disease follows. In this study, using a new mouse model with a liver-specific mutation of *Vps33b,* the mouse version of a gene that is mutated in most patients with arthrogryposis, renal dysfunction and cholestasis (ARC) syndrome, we investigated how the *Vps33b* gene product contributes to establishing hepatocyte polarity. We identified in these mice abnormalities similar to those in children with ARC syndrome. Gene transfer could partly reverse the mouse abnormalities. Our work contributes to the understanding of *VPS33B* disease and hepatocyte polarity in general, and may point toward gene transfer mediated treatment of ARC liver disease.

Graphical Abstract

Introduction

In metazoans, the development of three dimensional body structures depends on the generation of polarised epithelial layers. Polarisation of epithelial cells is a complex process that requires the cooperation of multiple factors including cell junction formation, extracellular matrix interactions and intracellular protein trafficking (1). Correct interaction of these factors enables the establishment of discrete apical and basolateral membrane domains. This then promotes normal epithelial cell function by allowing directional solute absorption and secretion (2).

In hepatocytes, the basolateral membrane faces sinusoidal blood and one or more apical domains contribute to the formation of bile canaliculi in conjunction with adjacent hepatocytes. This polarisation enables the directional flow of molecules from sinusoidal blood to canalicular bile and, as such, is crucial for normal biliary physiology (3). Genetic disorders of hepatic tight junction formation and protein trafficking entail a loss of hepatocyte polarity. This impaired hepatocyte polarity causes pathophysiological features similar to those of cholestatic liver diseases caused by mutations in genes encoding apical ATP-binding cassette transporters (4-7).

One such polarity-loss disorder is arthrogryposis renal dysfunction and cholestasis syndrome (ARC). ARC is an autosomal recessive multisystem disorder. It has a spectrum of severity and typically is characterised by congenital joint contractures, renal tubular acidosis and neonatal jaundice leading to death in infancy (8).

However, in milder cases patients survive into adulthood and have raised serum bile acid values but normal bilirubin levels (9). Approximately 75% of ARC patients harbour germline mutations in *VPS33B*. VPS33B is orthologous to the yeast Sec-1-Munc18 family protein Vps33p: a class C vacuolar protein sorting (vps) protein that regulates SNARE-mediated vesicle fusion (10). Class C vps proteins are core constituents of the HOPS (homotypic fusion and vacuole protein sorting) and CORVET (class C core vacuole/endosome tethering) multiprotein complexes, crucial in several stages of vesicular trafficking (11). Whilst the Vps33p ortholog VPS33A is recognised as a member of the mammalian HOPS complex (12), the function of VPS33B is associated with the activity of Rab11 family members (13).

Rab11a is involved in protein trafficking via the apical recycling endosome (ARE) and, thereby, biogenesis of the apical membrane domain (14). Canalicular proteins that are specifically trafficked via Rab11a-positive ARE are mislocalised in ARC patient liver (8, 11). Whilst patients' serum aminotransferase and gamma-glutamyl transpeptidase (ɣGT) activities are normal, serum alkaline phosphatase (ALP) activity is substantially elevated (8).

To treat the human liver diseases associated with failure to regulate apical-basolateral polarity, one must understand the pathways that govern hepatocyte polarisation. We therefore investigated the molecular pathology of ARC liver disease to elucidate the role of VPS33B in establishing hepatocyte polarity in mammals. We generated and characterised a novel murine model with a liver-specific *Vps33b* gene mutation (*Vps33b*$^{fl/fl}$*-AlfpCre*) that recapitulates key aspects of ARC liver disease. In *Vps33b*$^{fl/fl}$*-AlfpCre* animals we observed structural and functional defects of hepatocyte polarity associated with failure to generate the canalicular membrane

correctly. We could, in part, reverse these defects by adeno-associated virus mediated gene transfer.

Materials and methods

Vps33b$^{fl/fl}$*-AlfpCre* mouse generation

Mice with *Vps33b* exons 2-3 flanked by loxP sites were generated by Artemis Pharmaceuticals (Cologne, Germany) as described and crossed onto a C57BL/6J background (15). Mice were further crossed with AlfpCre-recombinase expressing animals to obtain *Vps33b*$^{fl/fl}$*-AlfpCre* mice with hepatocyte and cholangiocyte specific *Vps33b* deletion (16). Animals were sacrificed at 14-16 weeks of age and Cre-negative, age matched littermates were used as wild type controls. For experiments on a CA diet, 8 week old mice were fed 0.5% CA supplemented chow (TestDiet® Europe, London, UK) for 6 weeks and sacrificed immediately thereafter at age 14 weeks. For histologic assessment in older animals, mice were aged for 10 to 12 months and fed a normal chow diet. All experimental animal groups were of mixed gender. All procedures were undertaken with United Kingdom Home Office approval in accordance with the Animals (Scientific Procedures) Act of 1986.

Mass spectrometry

Bile acids were quantified by UPLC-MS/MS (17). Bile acid concentrations in bile were corrected by flow rate. Details are provided in the supplemental methods section.

Transmission electron microscopy (TEM)

Details of TEM procedures (13) are provided in the supplemental methods section.

Biliary secretion analysis

For analysis of bile composition, bile was collected by cannulating the gall bladder of 14-16 week old cholic acid (CA) fed mice using polyethylene (PE-10) tubing following midline laparotomy and ligation of the common bile duct. Analysis of biliary cholyl-L-lysyl-fluorescein (CLF) secretion via MRP2 was carried out using *in vivo* methods (18). Integrity of hepatic tight junction barrier function was measured using 40KDa fluorescein isothiocyanate (FITC)-conjugated dextran (FD-40) (19). Results obtained from CLF and FD-40 fluorometric analysis were corrected for bile flow rate.

Microarray analysis

Total RNA was extracted from liver samples using the RNAeasy Microkit per manufacturer' instructions (Qiagen, Manchester, UK). RNA transcript levels were measured using Affymetrix Mouse Gene 2.0 microarrays. Details of *in silico* gene expression and pathway analysis are described in the supplemental methods section.

The data discussed in this publication have been deposited in NCBI's Gene Expression Omnibus (20) and are accessible through GEO series accession number GSE83192.

(https://www.ncbi.nlm.nih.gov/geo/query/acc.cgi?acc=GSE83192)

AAV vector production

All ssAAV2/8 vectors were made by the adenovirus-free transient transfection method, using a chimeric AAV2 Rep-8Cap packaging plasmid (pAAV2-8) and an adenoviral helper plasmid (21). Vectors were purified (22) and vector genome (vg) titres were determined by standard alkaline gel based methods (23). Details of molecular cloning procedures are provided in the supplemental methods section.

Serum and bile biochemical assays, immunoblotting and histological and immunostaining procedures are described in the supplemental methods section.

Results

The ARC liver phenotype is recapitulated in *Vps33b$^{fl/fl}$-AlfpCre* mice and exacerbated by CA feeding.

Loss of *Vps33b* expression in hepatocytes of *Vps33b$^{fl/fl}$-AlfpCre* animals was confirmed by fluorescence *in situ* hybridisation and western blotting techniques (supplementary figure 1A and B).

To assess hepatobiliary injury associated with *Vps33b* mutation, levels of plasma alkaline phosphatase (ALP) activity; ALT activity and bilirubin concentrations were measured in 14-week-old animals fed normal chow or a 0.5% CA diet (n=4-6). As in ARC patients, a significant increase in plasma ALP activity was detected in normal chow fed *Vps33b$^{fl/fl}$-AlfpCre* mice (3-fold, median 241.0U/L, IQR 123.5-283.5U/L) in comparison to Cre-negative *Vps33b$^{fl/fl}$* littermates (median 80.0U/L, IQR 54.0-113.50U/L) (Figure 1A, P=0.0317, Mann Whitney U test). In CA fed animals, a greater increase in ALP activity (6.5-fold) was observed in the plasma of *Vps33b$^{fl/fl}$-AlfpCre* mice (median 874.5U/L, IQR 688.0-994.5U/L) than in that of *Vps33b$^{fl/fl}$* mice

(median 134.0U/L, IQR 108-144.0U/L) (Figure 1A, P=0.0022, Mann Whitney U test). Whilst ALT activity levels appeared slightly raised in *Vps33b*$^{fl/fl}$*-AlfpCre* animals, no significant difference in plasma ALT activity was found between *Vps33b*$^{fl/fl}$ and *Vps33b*$^{fl/fl}$*-AlfpCre* mice under both diet conditions (Figure 1B, normal diet P=0.0591, CA diet P=0.1775, Mann Whitney U test). Although ALT activity levels increased in both *Vps33b*$^{fl/fl}$ and *Vps33b*$^{fl/fl}$*-AlfpCre* animals following CA feeding, this increase was not statistically significant (*Vps33b*$^{fl/fl}$ P=0.0691, *Vps33b*$^{fl/fl}$*-AlfpCre* P=0.1111). Addition of CA to the diet may therefore have a slight effect on liver injury in both wild type and knockout animals. CA feeding consistently increased liver mass in *Vps33b*$^{fl/fl}$ and *Vps33b*$^{fl/fl}$*-AlfpCre* mice (1.5-fold, *Vps33b*$^{fl/fl}$ P=0.0078, *Vps33b*$^{fl/fl}$*-AlfpCre* P=0.0043) and liver mass was significantly increased between *Vps33b*$^{fl/fl}$ and *Vps33b*$^{fl/fl}$*-AlfpCre* mice under both diet conditions (normal diet 1.7-fold; P=0.0117, CA diet 1.5-fold; P=0.0050) (Figure 1C). Plasma bilirubin concentrations were below detection level (<2µmol/L) in all experimental groups.

As high plasma bile acid levels characterise ARC cholestasis (8), we measured bile acids in mouse plasma by mass spectrometry (n=5-6). Concordantly, median total bile acid levels of 97.30µM (IQR 68.85-259.2µM) and 12.65µM (IQR 7.65-20.90µM) were observed in normal diet *Vps33b*$^{fl/fl}$*-AlfpCre* and *Vps33b*$^{fl/fl}$ samples respectively (Figure 1D, 7.6-fold, P=0.0043, Mann Whitney U test). In CA diet *Vps33b*$^{fl/fl}$*-AlfpCre* and *Vps33b*$^{fl/fl}$ plasma samples, total bile acid levels were increased with respective concentrations of 190.4µM (IQR 78.2-295.9µM) and 24.1µM (IQR 13.0-31.9µM) detected (7.9-fold, P=0.0022).

These results collectively show that key biomarkers of ARC cholestasis (raised plasma ALP and bile acid levels, with normal aminotransferase levels) are recapitulated in *Vps33b*$^{fl/fl}$*-AlfpCre* mice fed either normal chow or a 0.5% CA diet.

As CA feeding did not create artefactual phenotypes in *Vps33b*$^{fl/fl}$*-AlfpCre* mice and only exacerbated disease phenotypes already observed at physiological level, CA feeding was not considered a confounding factor. The remaining experiments in this study were carried out in CA fed animals unless otherwise stated.

Histologic Findings in Livers of *Vps33b*$^{fl/fl}$*-AlfpCre* mice

Light microscopy of 14-week-old, CA fed *Vps33b*$^{fl/fl}$*-AlfpCre* mouse liver sections primarily revealed fibrotic changes that were not observed in *Vps33b*$^{fl/fl}$ sections. By trichrome staining (n=3) we observed periportal and pericentral fibrous expansion with focal bridging fibrosis in *Vps33b*$^{fl/fl}$*-AlfpCre* mice (Figure 1E). As leucocyte infiltration was observed in *Vps33b*$^{fl/fl}$*-AlfpCre* liver (supplementary figure 2), these fibrotic changes may indicate a response to inflammation caused by cholestasis in *Vps33b*$^{fl/fl}$*-AlfpCre* animals.

Trichrome staining of liver sections from 12-month-old *Vps33b*$^{fl/fl}$*-AlfpCre* mice fed normal chow revealed marked geographic fibrosis and focal steatosis (n=3) (Figure 1E). This suggests a progression of fibrotic changes and possible defects of lipid metabolism and accumulation in aged animals.

To investigate the mechanism of liver damage in *Vps33b*$^{fl/fl}$*-AlfpCre* mice, levels of apoptosis were assessed by immunostaining 14-week-old liver sections to detect cleaved caspase 3 (CC3) protein (n=3). The percentage of CC3 positive cells per field of view was significantly increased in *Vps33b*$^{fl/fl}$*-AlfpCre* sections in comparison to *Vps33b*$^{fl/fl}$ sections under both normal diet and CA diet conditions (P=<0.0001 and P=0.0058 respectively, Mann Whitney U test) (supplementary figure 3). This suggests that apoptosis may contribute to the liver injury observed in *Vps33b*$^{fl/fl}$*-AlfpCre* mice. However, in comparison to cholestatic mouse models of bile salt

export pump (BSEP) deficiency, the percentage of apoptotic cells detected in *Vps33b*$^{fl/fl}$*-AlfpCre* sections was relatively low (24).

Vps33b$^{fl/fl}$*-AlfpCre* animals show mislocalisation of apical membrane proteins

In vitro studies have suggested that VPS33B has a role in apical membrane protein trafficking in epithelial cells (11). This is reported specifically to involve interaction with Rab11a-positive ARE. To investigate possible defects of protein trafficking to the canalicular membrane, we used immunostaining of *Vps33b*$^{fl/fl}$ and *Vps33b*$^{fl/fl}$*-AlfpCre* mouse liver sections to assess the localisation of apical membrane proteins known to be trafficked via Rab11a-positive ARE (n=3). In contrast to *Vps33b*$^{fl/fl}$ tissue, in *Vps33b*$^{fl/fl}$*-AlfpCre* sections we observed absence of the ATP-binding cassette proteins BSEP and ABCG8 at the hepatocyte canalicular membrane (Figure 2A and supplementary figure 4A). These proteins are responsible for secretion into bile of conjugated bile acids and cholesterol respectively (25-27). We also observed mislocalisation of the GPI anchored glycoprotein carcinoembryonic antigen (CEA) in *Vps33b*$^{fl/fl}$*-AlfpCre* liver with a diffuse stain appearing around the entire hepatocyte membrane as opposed to the clear and selective apical marking in *Vps33b*$^{fl/fl}$ liver (supplementary figure 4b). Multidrug resistance-associated protein 2 (MRP2) reportedly bypasses the RE during apical trafficking (28, 29). Interestingly, as in ARC patients, MRP2 did not appear mislocalised in *Vps33b*$^{fl/fl}$*-AlfpCre* mouse liver (Figure 2B). Localisation of basolateral proteins appeared unaffected by loss of *Vps33b* (supplementary figure 4C).

Immunofluorescence detection of BSEP in normal chow fed mice established that protein mislocalisation was not an artefact of CA feeding and also showed

intracellular punctate staining in *Vps33b*$^{fl/fl}$*-AlfpCre* sections (supplementary figure 5A). Immunoblotting analysis showed that BSEP and ABCG8 expression levels were not strongly affected in *Vps33b*$^{fl/fl}$*-AlfpCre* liver (supplementary figure 5B and 5C). These data collectively suggest that canalicular proteins were mislocalised to intracellular vesicles rather than down-regulated in *Vps33b*$^{fl/fl}$*-AlfpCre* liver.

Disruption of functional hepatocyte polarity in *Vps33b*$^{fl/fl}$*-AlfpCre* mice

To investigate the physiological impact of apical protein mislocalisation, levels of bile components were assessed by mass spectrometry in plasma and bile samples of CA fed *Vps33b*$^{fl/fl}$ and *Vps33b*$^{fl/fl}$*-AlfpCre* mice (n=4-6). We observed a significant increase in plasma bile salt levels of *Vps33b*$^{fl/fl}$*-AlfpCre* animals over those of *Vps33b*$^{fl/fl}$ mice (Table 1). The major accumulating bile acid in plasma was taurocholate, which in *Vps33b*$^{fl/fl}$*-AlfpCre* mice was present at a median concentration of 97.9 µM: 49-fold higher than the median concentration in *Vps33b*$^{fl/fl}$ mice. The median concentrations of most other bile acid species were also increased: glycocholate 9.7-fold; cholate 7-fold; tauro-diOH-cholanoates 7.5-fold; glyco-diOH-cholanoates 9.3-fold; tauro-tetraOH-cholanoates 80-fold; glyco-tetraOH-cholanoates 26-fold.

In comparison to *Vps33b*$^{fl/fl}$ mice, the main biliary bile acid, taurocholate, was present at 1.9-fold higher concentrations in *Vps33b*$^{fl/fl}$*-AlfpCre* mouse bile (not statistically significant). Biliary levels of glyco-diOH-cholanoates were equivalent between *Vps33b*$^{fl/fl}$*-AlfpCre* and *Vps33b*$^{fl/fl}$ animals (Table 2). However, median biliary concentrations of all other bile acids were lower in *Vps33b*$^{fl/fl}$*-AlfpCre* mice than in *Vps33b*$^{fl/fl}$ mice (1.9-, 13.3-, 1.5- and 4.3-fold reduction in glycocholate, unconjugated cholate, tauro-diOH-cholanoates, and unconjugated diOH-cholanoates respectively).

These reduced concentrations were not statistically significant excepting unconjugated cholate (P=0.0190).

Total cholesterol and phospholipid levels were also significantly increased in plasma (2.8- and 2-fold respectively) and decreased in bile (3.6- and 1.5-fold respectively) of *Vps33b*$^{fl/fl}$*-AlfpCre* animals (P=0.0079 in all tests, Mann Whitney test) (Figure 2C and 2D). Collectively these results suggest that the directional flow of bile components from blood to canalicular bile is disrupted in *Vps33b*$^{fl/fl}$*-AlfpCre* mice. Increased levels of plasma total cholesterol were confirmed in normal chow fed *Vps33b*$^{fl/fl}$*-AlfpCre* (supplementary figure 6A).

In a further group of 14-week-old CA fed animals, we analysed the composition of plasma cholesterol as concentrations of total (supplementary figure 6B), free and esterified cholesterol (n=6-7). Levels of free cholesterol in plasma of *Vps33b*$^{fl/fl}$*-AlfpCre* mice were significantly increased (3.6-fold; P=0.0012, Mann Whitney U test) over those of *Vps33b*$^{fl/fl}$ animals (supplementary figure 6C, median 0.3678µg/µl; IQR 0.2996-0.5072µg/µl and median 0.1036µg/µl; IQR 0.0836-0.1615µg/µl respectively) whilst levels of esterified cholesterol were equivalent between *Vps33b*$^{fl/fl}$*-AlfpCre* and *Vps33b*$^{fl/fl}$ mice (supplementary figure 6D, median 0.5134 µg/µl; IQR 0.3869-0.5459 µg/µl and median 0.4371µg/µl ; IQR 0.3998-0.5747 µg/µl respectively). This suggests that the increased levels of total cholesterol observed in plasma of *Vps33b*$^{fl/fl}$*-AlfpCre* mice are largely due to the increase in concentration of free cholesterol as opposed to esterified cholesterol.

Cholyl-L-lysyl fluorescein (CLF) is secreted into canalicular bile specifically via MRP2 (18). To determine whether MRP2 protein was functional as well as correctly localised in *Vps33b*$^{fl/fl}$*-AlfpCre* hepatocytes, anaesthetised animals were given an intravenous injection of CLF followed by collection of bile and plasma fractions for fluorometric quantification of CLF (n=4). Plasma and bile levels of CLF did not significantly differ between *Vps33b*$^{fl/fl}$*-AlfpCre* and *Vps33b*$^{fl/fl}$ mice, suggesting normal MRP2 function in V*ps33b* deficiency (Figure 2E and 2F). However, accumulation of CLF in bile appeared more rapid in *Vps33b*$^{fl/fl}$*-AlfpCre* animals. This is consistent with reports that suggest an increase in mouse MRP2 expression levels in liver in response to bile acid retention (30).

Inflammatory and metabolic pathways are perturbed in *Vps33b*$^{fl/fl}$*-AlfpCre* liver

To assess differential gene expression in liver following *Vps33b* deletion, we carried out microarray analysis of total RNA isolated from *Vps33b*$^{fl/fl}$ and *Vps33b*$^{fl/fl}$*-AlfpCre* liver samples (n=4-6) from mice fed a 0.5% CA diet and sacrificed at 10-14 weeks.

Using partial least squares (PLS) regression, we observed that the first PLS component clearly separated *Vps33b*$^{fl/fl}$*-AlfpCre* from *Vps33b*$^{fl/fl}$ liver samples (supplementary figure 7). Relevant genes were identified by selecting those with the largest contribution to the first component (Figure 3).

In comparison to samples from Cre-negative littermates, in *Vps33b*$^{fl/fl}$*-AlfpCre* liver, we observed upregulation of several genes involved in the inflammatory response. This included markers of immune cells (*Ly6d*, *Cd14*) as well as chemokines that induce immune cell infiltration (*Ccl2, Cxcl10*). Using the Database for Annotation, Visualization and Integrated Discovery (DAVID), we identified many over-represented gene ontology (GO) annotations in the top 150 genes (supplementary

figure 8). In particular we observed terms relating to 'inflammatory response' but annotations such as 'membrane' and 'extracellular region' were also elicited.

Additionally, numerous genes involved in metabolic pathways were identified as misregulated in *Vps33b*$^{fl/fl}$*-AlfpCre* mouse liver. Gene Set Enrichment Analysis (GSEA) consistently identified the Kegg pathway bile acid biosynthesis as the most perturbed pathway in *Vps33b*$^{fl/fl}$*-AlfpCre* animals. Several other metabolic and inflammatory pathways also were perturbed (supplementary table 1).

Collectively, these data support our observations of inflammation and fibrotic changes in *Vps33b*$^{fl/fl}$*-AlfpCre* liver and suggests that intrahepatic retention of bile components may directly result in dysregulation of bile acid metabolism in *Vps33b*$^{fl/fl}$*-AlfpCre* mice.

The hepatocyte phenotype is rescued by AAV mediated gene transfer

To determine whether reintroduction of VPS33B to *Vps33b*$^{fl/fl}$*-AlfpCre* hepatocytes could restore structural and functional polarity, we performed gene transfer experiments using ssAAV2/8 vectors containing either wild type or codon optimised human *VPS33B* cDNA (ssAAV2/8-EFS-*hVPS33B*-WPRE and ssAAV2/8-EFS-*hVPS33Bco*-WPRE respectively) (Figure 4A). Vectors were administered to 5 week old mice at a dose of 1×10^{12} vector genomes (vg) per animal via intraperitoneal injection. At 8 weeks of age, injected animals and control groups received CA supplemented feed for 6 weeks. At 14 weeks, without re-exposure to a normal diet, animals were sacrificed and transgene expression in hepatocytes was confirmed immunohistochemically (supplementary figure 9).

In animals treated with ssAAV2/8-EFS-*hVPS33B*-WPRE and ssAAV2/8-EFS-*hVPS33Bco*-WPRE vectors, we observed respective 2.1- and 4.9-fold decreases in median levels of plasma ALP versus *Vps33b*$^{fl/fl}$*-AlfpCre* mice (Figure 4B). This was accompanied by a 2.7-fold decrease of total plasma bile acid levels in ssAAV2/8-EFS-*hVPS33B*-WPRE treated mice and a significant 11-fold decrease in plasma bile acid levels of mice receiving ssAAV2/8-EFS-*hVPS33Bco*-WPRE (P=0.0015, Kruskal-Wallis test) (Figure 4C). Plasma levels of cholesterol and phospholipid were also reduced in mice receiving ssAAV2/8-EFS-*hVPS33B*-WPRE and ssAAV2/8-EFS-*hVPS33Bco*-WPRE vectors (Figures 4D and 4E).

Immunostaining demonstrated partial restoration of canalicular membrane protein localisation following gene transfer with both vectors (Figure 4F and supplementary figure 10). This suggests that, following gene transfer, functional polarity is rescued, as manifest by correction of protein localisation to the apical membrane.

Vps33b$^{fl/fl}$*-AlfpCre* hepatocytes show tight junction defects

Hepatic tight junctions constitute the barrier that separates sinusoidal blood from canalicular bile. Following knockdown of Rab11a, WIF-B9 cells form tight junctions that appear morphologically abnormal (31). To study the role of *Vps33b* in Rab11a dependent canalicular membrane biogenesis, we investigated tight junction abnormalities in *Vps33b*$^{fl/fl}$*-AlfpCre* liver by immunostaining for Claudin1. In control *Vps33b*$^{fl/fl}$ liver, Claudin1 staining revealed normal belt-like tight junctions (Figure 5A). In *Vps33b*$^{fl/fl}$*-AlfpCre* tissue, Claudin1 marking was irregular and tortuous, suggesting changes in tight junction organisation (Figure 5B). Following gene transfer of 1×10^{12}vg/animal ssAAV2/8-EFS-*hVPS33Bco*-WPRE vector, we observed partial correction of tight junction appearance (Figure 5C).

To assess functional integrity of hepatic tight junctions in *Vps33b*$^{fl/fl}$*-AlfpCre* and *Vps33b*$^{fl/fl}$ liver, we measured levels of FD-40 in bile following intravenous injection. Disruption of tight junction barrier function results in rapid biliary accumulation of FD-40. Fluorometry documented build-up of FD-40 in the bile of *Vps33b*$^{fl/fl}$*-AlfpCre* mice earlier than in control *Vps33b*$^{fl/fl}$ littermates (P=0.01342) (Figure 5D). This observation suggests that tight junctions in *Vps33b*$^{fl/fl}$*-AlfpCre* mice, abnormal in Claudin1 distribution on immunostaining, were defective in function.

Structural abnormalities of *Vps33b*$^{fl/fl}$*-AlfpCre* canaliculi

Ultrastructure of *Vps33b*$^{fl/fl}$*-AlfpCre* and *Vps33b*$^{fl/fl}$ canaliculi was assessed by TEM. Relative to Cre-negative littermates, we observed a marked paucity of canalicular microvilli in *Vps33b*$^{fl/fl}$*-AlfpCre* hepatocytes (Figure 6A and 6B). Ultrastructure of the bile canaliculi appeared restored in mice treated with ssAAV2/8-EFS-*hVPS33Bco*-WPRE vector (Figure 6C). To quantify these observations in terms of apical membrane length relative to canaliculus size, we measured the total inner membrane length of the bile canaliculi and normalised these values to the length of the outer canalicular perimeter (Figure 6D). In *Vps33b*$^{fl/fl}$*-AlfpCre* cells we observed a significant decrease in inner membrane length in comparison to Vps33b$^{fl/fl}$ cells. This corresponds to an overall loss of canalicular membrane surface area in the absence of *Vps33b*. This observation was accompanied by a significant increase in canalicular membrane length in hepatocytes of AAV treated mice in comparison to untreated *Vps33b*$^{fl/fl}$*-AlfpCre* animals (P<0.001, One way ANOVA, Bonferroni's test). Measurements of tight junction length and breadth did not differ between *Vps33b*$^{fl/fl}$ and *Vps33b*$^{fl/fl}$*-AlfpCre* micrographs (supplementary figure 11).

Discussion

Loss of apical-basolateral hepatocyte polarity is observed in many types of inherited cholestatic liver disease and in liver cancer (4-7, 32, 33). However, the molecular mechanisms that cause this loss are not well determined. In this study, we aimed to improve understanding of the pathways that govern hepatocyte polarity. Specifically, we investigated the role of VPS33B in biogenesis of the bile canaliculus and subsequent maintenance of apical domain structure and function. To achieve this aim, we generated a novel murine model with a liver epithelial cell-specific deletion of *Vps33b* (*Vps33b*$^{fl/fl}$*-AlfpCre*) that recapitulates hepatocyte polarity defects observed in patients with ARC syndrome.

ARC patients with *VPS33B* mutations show cholestasis with high plasma ALP activity and bile acid levels. Patients' aminotransferase activity and ɣGT levels remain normal (8). In agreement with these data, our *Vps33b*$^{fl/fl}$*-AlfpCre* mice demonstrated significant increases in plasma ALP and total bile acid levels in comparison to Cre-negative littermates. As seen in other cholestasis models, these phenotypes were exacerbated by CA feeding (34). No significant difference in plasma ALT activity was observed in *Vps33b*$^{fl/fl}$*-AlfpCre* versus *Vps33b*$^{fl/fl}$ mice and ɣGT levels were not assessed as mice do not express ɣGT in hepatocytes after birth (35). Biomarkers in our *Vps33b*$^{fl/fl}$*-AlfpCre* mouse thus accurately track those used to assess ARC liver disease. Like patients with clinically milder ARC, *Vps33b*$^{fl/fl}$*-AlfpCre* animals did not manifest increased serum bilirubin levels.

As ALP is normally expressed at the apical hepatocyte membrane, the increase in plasma ALP levels in *Vps33b*$^{fl/fl}$*-AlfpCre* animals may be due to defects in apical membrane biosynthesis. Further increases in plasma ALP caused by the CA diet may be related to canalicular damage, although increased ALP synthesis or shifts in localisation are also possible. Further evidence of canalicular injury is supplied by

immunostaining of ARC patient liver biopsy specimens, which reveals mislocalisation of proteins typically located at the apical membrane. Among these is BSEP, an ATP binding cassette transporter required for movement of conjugated bile acids from blood to bile (25). The mislocalisation of BSEP was reproduced in our *Vps33b*$^{fl/fl}$-*AlfpCre* animals under both normal diet and CA diet conditions. By immunofluorescence, we observed punctate intracellular BSEP staining, consistent with localisation of BSEP in intracellular vesicles.

In patients with progressive familial intrahepatic cholestasis type 2 (PFIC2), the loss of BSEP results in intrahepatic retention of bile salts (36). In the *Bsep* knockout mouse, severe cholestatic liver disease is observed when mice are fed a diet containing 0.5% CA (24). In agreement with these observations, by utilising a recently developed mass spectrometry technique, we detected significant increases (7 to 80-fold) in plasma concentrations of TCA, GCA, CA, tauro-diOH-cholanoates, glyco-diOH-cholanoates, tauro-tetraOH-cholanoates and glyco-tetraOH-cholanoates in *Vps33b*$^{fl/fl}$-*AlfpCre* mice fed 0.5% CA. Concentrations of plasma bile acids in *Vps33b*$^{fl/fl}$-*AlfpCre* animals were only slightly lower than values previously observed in the *Bsep* knockout mouse (24).

Our comparison of biliary bile acid concentrations in *Vps33b*$^{fl/fl}$-*AlfpCre* and *Vps33b*$^{fl/fl}$ mice also yielded results similar to those obtained on comparison of *Bsep* knockout and wild type mice (24). Neither the concentration of the major biliary bile acid component, taurocholate, nor the total biliary bile acid concentration differed significantly between *Vps33b*$^{fl/fl}$-*AlfpCre* and *Vps33b*$^{fl/fl}$ animals. This may indicate an alternative route of apical bile acid secretion following CA feeding such as via MRP2 (37). For some of the lesser bile acids, biliary concentrations were lower in *Vps33b*$^{fl/fl}$-*AlfpCre* mice than in *Vps33b*$^{fl/fl}$ mice. This reduction in biliary concentration

was statistically significant only in the case of unconjugated cholate. As in the *Bsep* knockout mouse, this may indicate a higher rate of taurine conjugation and conversion to tetra-OH bile acid species in *Vps33b*$^{fl/fl}$*-AlfpCre* animals as a mechanism of reducing bile acid toxicity (38). Indeed, the proportion of unconjugated bile acids in plasma and bile of *Vps33b*$^{fl/fl}$*-AlfpCre* mice was lower than that of *Vps33b*$^{fl/fl}$ littermates and a significant increase in conjugated tetra-OH species was observed in *Vps33b*$^{fl/fl}$*-AlfpCre* plasma. Overall, this data suggest that mislocalisation of BSEP in *Vps33b*$^{fl/fl}$*-AlfpCre* mice has a similar effect on transport of bile acids to the effect of *Bsep* knockout. However, even CA fed *Vps33b*$^{fl/fl}$*-AlfpCre* animals had normal serum bilirubin concentrations, no obvious reduction in survival and only a small increase in apoptosis (as detected by CC3 staining), thus suggesting liver disease less severe than that in *Bsep* knockout mice (24).

In addition to BSEP mislocalisation, in *Vps33b*$^{fl/fl}$*-AlfpCre* hepatocytes we observed mislocalisation of ABCG8, an apical ATP-binding cassette transporter involved in the directional movement of cholesterol (27). Concordant with a loss of apical ABCG8, in comparison to *Vps33b*$^{fl/fl}$ mice, we detected reduced levels of total cholesterol in bile and accumulation of cholesterol in plasma of CA fed *Vps33b*$^{fl/fl}$*-AlfpCre* animals. Collectively these results suggest that, in the absence of *Vps33b*, apical transporter proteins are mislocalised, causing an overall loss of functional polarity and accumulation of bile components in blood.

Interestingly, the increase in plasma total cholesterol observed in *Vps33b*$^{fl/fl}$*-AlfpCre* animals was due to an increase in free cholesterol as opposed to esterified cholesterol. In combination with our observation of canalicular proteins mislocalised to possible intracellular vesicles, as in other cholestatic models, this increase in free cholesterol may imply that the majority of phospholipid and cholesterol in *Vps33b*$^{fl/fl}$-

AlfpCre plasma is present in the form of lipoprotein X, biliary lipid vesicles that contain mostly free cholesterol and phosphatidylcholine, ascribed in cholestasis to shedding of hepatocyte membranes into bile and thence, with bile, between hepatocytes into plasma (39, 40).

Proteins that appear mislocalised in *Vps33b$^{fl/fl}$-AlfpCre* mouse hepatocytes are thought to be trafficked to the canalicular membrane specifically via Rab11a-positive ARE (41). In our model we observed mislocalisation of apical proteins that are trafficked directly from the trans golgi network (TGN) to the ARE (BSEP and ABCG8) as well as proteins that are first delivered to the basolateral membrane from TGN and then transcytosed to the canalicular membrane via ARE (CEA) (41). However, as in ARC patients, MRP2 was not mislocalised in *Vps33b$^{fl/fl}$-AlfpCre* liver. MRP2 is reported to bypass Rab11a-positive recycling ARE en route to the hepatocyte apical domain (28, 29). Functional integrity of MRP2 in *Vps33b$^{fl/fl}$-AlfpCre* liver was confirmed by intravenous administration and subsequent quantification in bile of cholyl-lysyl-fluorescein (a compound specifically exported into bile via MRP2) (18). As in zebrafish, these results suggest that mammalian VPS33B is specifically involved in trafficking of proteins to the apical domain via Rab11a-positive ARE (11). Basolateral membrane proteins were not mislocalised in *Vps33b$^{fl/fl}$-AlfpCre* hepatocytes, suggesting a specific role for VPS33B in biogenesis of the bile canaliculus.

As we observed in mutant mice that MRP2 is functional and normally sited, as is MRP2 in ARC patients (11), we infer that the collections of Dubin-Johnson - like pigment in some ARC patients' hepatocytes (42) are unlikely to originate from MRP2 absence or dysfunction.

To assess defects in structural components of hepatocyte polarity, we analysed tight junction integrity in *Vps33b*$^{fl/fl}$*-AlfpCre* and *Vps33b*$^{fl/fl}$ liver. As in cultured cells, immunohistochemical marking for Claudin1, a tight junction component, was irregular in *Vps33b*$^{fl/fl}$*-AlfpCre* liver, with tortuous distribution (31). Tight junctions between control *Vps33b*$^{fl/fl}$ hepatocytes appeared uniform and belt-like. This suggestion of a structural tight junction defect was supported by our functional analysis of tight junction integrity which showed rapid accumulation of fluorescence in the bile of *Vps33b*$^{fl/fl}$*-AlfpCre* mice following intravenous injection of 40KDa fluorescent dextran (FD-40). The observed leaking of FD-40 from blood into bile suggests a loss of tight junction barrier function in *Vps33b*$^{fl/fl}$*-AlfpCre* hepatocytes (19). Whether tight junction proteins are normally trafficked to the apical membrane by VPS33B or loss of tight junction integrity is a secondary effect of incorrect apical protein trafficking remains to be determined. In contrast to reports in *Tjp2* knockout mice, our TEM analysis of tight junction ultrastructure revealed no overall increase in tight junction length or breadth following deletion of *Vps33b* (4, 7). In future studies, freeze fracture electron microscopy may be used for a more detailed assessment of tight junction composition in *Vps33b*$^{fl/fl}$*-AlfpCre* liver.

Analysis of ultrastructural images of *Vps33b*$^{fl/fl}$*-AlfpCre* liver revealed a significant reduction in apical membrane area due to a partial loss of canalicular microvilli. This implies a loss of structural polarity at the apical membrane and an overall reduction of surface area for movement of solutes from the hepatocyte into bile. When Rab11a is mutated in mouse intestine, apical brush border microvilli are lost (43). These results provide an interesting link between the observed interaction of VPS33B in Rab11a protein trafficking pathways and the maintenance of apical microvilli in hepatocytes.

To confirm the role of VPS33B in hepatocyte polarity, we performed *in vivo* gene rescue studies in *Vps33b*$^{fl/fl}$*-AlfpCre* mice using ssAAV2/8 vectors containing either wild type or codon optimised human *VPS33B* cDNA (ssAAV2/8-EFS-*hVPS33B*-WPRE and ssAAV2/8-EFS-*hVPS33Bco*-WPRE). At 9 weeks after gene transfer (1×10^{12}vg/mouse in 4-5 week old animals) we observed partial rescue of apical protein localisation, Claudin1 distribution at tight junctions, canalicular ultrastructure and plasma ALP activity, cholesterol, phospholipid and bile acid levels. This phenotype correction appeared more robust in animals treated with the codon optimised vector: all such animals had plasma total bile acid levels equivalent to those in control *Vps33b*$^{fl/fl}$ mice. As well as confirming that the observed loss of polarity in *Vps33b*$^{fl/fl}$*-AlfpCre* hepatocytes is due to *Vps33b* mutation, these experiments establish an initial proof of principle for future therapeutic use of gene transfer in ARC patients. To meet a therapeutic aim, dose optimisation and safety of *VPS33B* gene transfer would need to be determined in future studies.

In conclusion, using our novel *Vps33b*$^{fl/fl}$*-AlfpCre* mouse model, we have identified that VPS33B is vital for maintenance of mammalian structural and functional hepatocyte polarity. We have established that genetic hepatocyte polarity disorders can be rescued using gene transfer with AAV vectors and that ARC liver disease may be a potential target of therapeutic gene replacement.

Acknowledgements

We would like to thank the Great Ormond Street Hospital, Camelia Botnar Laboratories, chemical pathology services for contribution towards assessment of liver function. Histologic samples were imaged in the UCL Institute of Child Health Imaging Facility.

References

1. Treyer A, Musch A. Hepatocyte polarity. Compr Physiol 2013;3:243-287.

2. Cereijido M, Contreras RG, Shoshani L. Cell adhesion, polarity, and epithelia in the dawn of metazoans. Physiol Rev 2004;84:1229-1262.

3. Slim CL, Lazaro-Dieguez F, Bijlard M, Toussaint MJ, de Bruin A, Du Q, Musch A, et al. Par1b induces asymmetric inheritance of plasma membrane domains via LGN-dependent mitotic spindle orientation in proliferating hepatocytes. PLoS Biol 2013;11:e1001739.

4. Carlton VEH, Harris BZ, Puffenberger EG, Batta AK, Knisely AS, Robinson DL, Strauss KA, et al. Complex inheritance of familial hypercholanemia with associated mutations in TJP2 and BAAT. Nature Genetics 2003;34:91-96.

5. Girard M, Lacaille F, Verkarre V, Mategot R, Feldmann G, Grodet A, Sauvat F, et al. MYO5B and bile salt export pump contribute to cholestatic liver disorder in microvillous inclusion disease. Hepatology 2014;60:301-310.

6. Hadj-Rabia S, Baala L, Vabres P, Hamel-Teillac D, Jacquemin E, Fabre M, Lyonnet S, et al. Claudin-1 gene mutations in neonatal sclerosing cholangitis associated with ichthyosis: a tight junction disease. Gastroenterology 2004;127:1386-1390.

7. Sambrotta M, Strautnieks S, Papouli E, Rushton P, Clark BE, Parry DA, Logan CV, et al. Mutations in TJP2 cause progressive cholestatic liver disease. Nat Genet 2014;46:326-+.

8. Gissen P, Tee L, Johnson CA, Genin E, Caliebe A, Chitayat D, Clericuzio C, et al. Clinical and molecular genetic features of ARC syndrome. Hum Genet 2006;120:396-409.

9. Smith H, Galmes R, Gogolina E, Straatman-Iwanowska A, Reay K, Banushi B, Bruce CK, et al. Associations among genotype, clinical phenotype, and intracellular localization of trafficking proteins in ARC syndrome. Hum Mutat 2012;33:1656-1664.

10. Baker RW, Jeffrey PD, Zick M, Phillips BP, Wickner WT, Hughson FM. A direct role for the Sec1/Munc18-family protein Vps33 as a template for SNARE assembly. Science 2015;349:1111-1114.

11. Cullinane AR, Straatman-Iwanowska A, Zaucker A, Wakabayashi Y, Bruce CK, Luo G, Rahman F, et al. Mutations in VIPAR cause an arthrogryposis, renal dysfunction and cholestasis syndrome phenotype with defects in epithelial polarization. Nat Genet 2010;42:303-312.

12. Sriram V, Krishnan KS, Mayor S. deep-orange and carnation define distinct stages in late endosomal biogenesis in Drosophila melanogaster. J Cell Biol 2003;161:593-607.

13. Banushi B, Forneris F, Straatman-Iwanowska A, Strange A, Lyne AM, Rogerson C, Burden JJ, et al. Regulation of post-Golgi LH3 trafficking is essential for collagen homeostasis. Nat Commun 2016;7:12111.

14. Roland JT, Bryant DM, Datta A, Itzen A, Mostov KE, Goldenring JR. Rab GTPase-Myo5B complexes control membrane recycling and epithelial polarization. Proc Natl Acad Sci U S A 2011;108:2789-2794.

15. Bem D, Smith H, Banushi B, Burden JJ, White IJ, Hanley J, Jeremiah N, et al. VPS33B regulates protein sorting into and maturation of alpha-granule progenitor organelles in mouse megakaryocytes. Blood 2015;126:133-143.

16. Kellendonk C, Opherk C, Anlag K, Schutz G, Tronche F. Hepatocyte-specific expression of Cre recombinase. Genesis 2000;26:151-153.

17. Mazzacuva F, Mills P, Mills K, Camuzeaux S, Gissen P, Nicoli ER, Wassif C, et al. Identification of novel bile acids as biomarkers for the early diagnosis of Niemann-Pick C disease. FEBS Lett 2016; 11:1651-62.

18. de Waart DR, Hausler S, Vlaming ML, Kunne C, Hanggi E, Gruss HJ, Oude Elferink RP, et al. Hepatic transport mechanisms of cholyl-L-lysyl-fluorescein. J Pharmacol Exp Ther 2010;334:78-86.

19. Han X, Fink MP, Uchiyama T, Yang R, Delude RL. Increased iNOS activity is essential for hepatic epithelial tight junction dysfunction in endotoxemic mice. Am J Physiol Gastrointest Liver Physiol 2004;286:G126-136.

20. Edgar R, Domrachev M, Lash AE. Gene Expression Omnibus: NCBI gene expression and hybridization array data repository. Nucleic Acids Res 2002;30:207-210.

21. Nathwani AC, Davidoff A, Hanawa H, Zhou JF, Vanin EF, Nienhuis AW. Factors influencing in vivo transduction by recombinant adeno-associated viral vectors expressing the human factor IX cDNA. Blood 2001;97:1258-1265.

22. Davidoff AM, Ng CY, Sleep S, Gray J, Azam S, Zhao Y, McIntosh JH, et al. Purification of recombinant adeno-associated virus type 8 vectors by ion exchange chromatography generates clinical grade vector stock. J Virol Methods 2004;121:209-215.

23. Fagone P, Wright JF, Nathwani AC, Nienhuis AW, Davidoff AM, Gray JT. Systemic errors in quantitative polymerase chain reaction titration of self-complementary adeno-associated viral vectors and improved alternative methods. Hum Gene Ther 2011.

24. Wang R, Lam P, Liu L, Forrest D, Yousef IM, Mignault D, Phillips MJ, et al. Severe cholestasis induced by cholic acid feeding in knockout mice of sister of P-glycoprotein. Hepatology 2003;38:1489-1499.

25. Gerloff T, Stieger B, Hagenbuch B, Madon J, Landmann L, Roth J, Hofmann AF, et al. The sister of P-glycoprotein represents the canalicular bile salt export pump of mammalian liver. J Biol Chem 1998;273:10046-10050.

26. Stieger B, Fattinger K, Madon J, Kullak-Ublick GA, Meier PJ. Drug- and estrogen-induced cholestasis through inhibition of the hepatocellular bile salt export pump (Bsep) of rat liver. Gastroenterology 2000;118:422-430.

27. Yu L, Li-Hawkins J, Hammer RE, Berge KE, Horton JD, Cohen JC, Hobbs HH. Overexpression of ABCG5 and ABCG8 promotes biliary cholesterol secretion and reduces fractional absorption of dietary cholesterol. J Clin Invest 2002;110:671-680.

28. Bandler PE, Westlake CJ, Grant CE, Cole SP, Deeley RG. Identification of regions required for apical membrane localization of human multidrug resistance protein 2. Mol Pharmacol 2008;74:9-19.

29. Nies AT, Keppler D. The apical conjugate efflux pump ABCC2 (MRP2). Pflugers Arch 2007;453:643-659.

30. Slitt AL, Allen K, Morrone J, Aleksunes LM, Chen C, Maher JM, Manautou JE, et al. Regulation of transporter expression in mouse liver, kidney, and intestine during extrahepatic cholestasis. Biochim Biophys Acta 2007;1768:637-647.

31. Wakabayashi Y, Dutt P, Lippincott-Schwartz J, Arias IM. Rab11a and myosin Vb are required for bile canalicular formation in WIF-B9 cells. Proc Natl Acad Sci U S A 2005;102:15087-15092.

32. **Taniguchi K, Roberts LR,** Aderca IN, Dong X, Qian C, Murphy LM, Nagorney DM, et al. Mutational spectrum of beta-catenin, AXIN1, and AXIN2 in hepatocellular carcinomas and hepatoblastomas. Oncogene 2002;21:4863-4871.

33. **Vilarinho S, Erson-Omay EZ,** Harmanci AS, Morotti R, Carrion-Grant G, Baranoski J, Knisely AS, et al. Paediatric hepatocellular carcinoma due to somatic CTNNB1 and NFE2L2 mutations in the setting of inherited bi-allelic ABCB11 mutations. J Hepatol 2014;61:1178-1183.

34. Yeh TH, Krauland L, Singh V, Zou B, Devaraj P, Stolz DB, Franks J, et al. Liver-specific beta-catenin knockout mice have bile canalicular abnormalities, bile secretory defect, and intrahepatic cholestasis. Hepatology 2010;52:1410-1419.

35. Gallagher BC, Rudolph DB, Hinton BT, Hanigan MH. Differential induction of gamma-glutamyl transpeptidase in primary cultures of rat and mouse hepatocytes parallels induction during hepatocarcinogenesis. Carcinogenesis 1998;19:1251-1255.

36. Evason K, Bove KE, Finegold MJ, Knisely AS, Rhee S, Rosenthal P, Miethke AG, et al. Morphologic findings in progressive familial intrahepatic cholestasis 2 (PFIC2): correlation with genetic and immunohistochemical studies. Am J Surg Pathol 2011;35:687-696.

37. Megaraj V, Iida T, Jungsuwadee P, Hofmann AF, Vore M. Hepatobiliary disposition of 3alpha,6alpha,7alpha,12alpha-tetrahydroxy-cholanoyl taurine: a substrate for multiple canalicular transporters. Drug Metab Dispos 2010;38:1723-1730.

38. **Zhang Y, Li F,** Patterson AD, Wang Y, Krausz KW, Neale G, Thomas S, et al. Abcb11 deficiency induces cholestasis coupled to impaired beta-fatty acid oxidation in mice. J Biol Chem 2012;287:24784-24794.

39. Elferink RP, Ottenhoff R, van Marle J, Frijters CM, Smith AJ, Groen AK. Class III P-glycoproteins mediate the formation of lipoprotein X in the mouse. J Clin Invest 1998;102:1749-1757.

40. Manzato E, Fellin R, Baggio G, Walch S, Neubeck W, Seidel D. Formation of lipoprotein-X. Its relationship to bile compounds. J Clin Invest 1976;57:1248-1260.

41. Gissen P, Arias IM. Structural and functional hepatocyte polarity and liver disease. J Hepatol 2015;63:1023-1037.

42. Nezelof C, Dupart MC, Jaubert F, Eliachar E. A lethal familial syndrome associating arthrogryposis multiplex congenita, renal dysfunction, and a cholestatic and pigmentary liver disease. J Pediatr 1979;94:258-260.

43. Sobajima T, Yoshimura S, Iwano T, Kunii M, Watanabe M, Atik N, Mushiake S, et al. Rab11a is required for apical protein localisation in the intestine. Biol Open 2014;4:86-94.

Author names in bold designate shared co-first authorship.

Tables

Table 1. Concentrations of bile acids in plasma from *Vps33b*$^{fl/fl}$ and *Vps33b*$^{fl/fl}$-*AlfpCre* mice fed 0.5% cholic acid. Contributions of individual bile acids to the total bile acid pool are listed as percentages in parenthesis. Abbreviations: CA, cholic acid; C, cholanoate; T, tauro; G, glyco; DiOH, dihydroxy; tetraOH, tetrahydroxy.

Plasma concentrations (μM)							
Bile acid	*Vps33b*$^{fl/fl}$			*Vps33b*$^{fl/fl}$-*AlfpCre*			Comparison
	Median	25th Percentile	75th Percentile	Median	25th Percentile	75th Percentile	P value (Mann Whitney)
TCA	1.99 (9.69%)	1.49	4.16	97.9 (54.55%)	46.2	183	0.002
GCA	1.09 (5.31%)	0.57	1.61	10.6 (5.91%)	6.99	24.4	0.002
CA	3.44 (16.75%)	2.19	5.84	24.2 (13.48%)	5.50	33.0	0.02
Tauro-diOH-C	1.98 (9.64%)	1.28	2.62	14.8 (8.25%)	5.67	25.4	0.004
Glyco-diOH-C	0.08 (0.39%)	0.038	0.15	0.74 (0.41%)	0.20	2.30	0.002
DiOH-C	11.8 (57.45%)	5.41	19.9	24.0 (13.37%)	11.8	33.4	0.13 (ns)
Tauro-tetraOH-C	0.08 (0.39%)	0.068	0.16	6.40 (3.57%)	1.77	10.8	0.0048
Glyco-tetraOH-C	0.03 (0.15%)	0.018	0.057	0.78 (0.43%)	0.64	2.68	0.0238
TetraOH-C	0.05 (0.23%)	0.03	0.058	0.06 (0.03%)	0.03	0.09	0.5097 (ns)

Table 2. Concentrations of bile acids in bile from *Vps33b*$^{fl/fl}$ and *Vps33b*$^{fl/fl}$*-AlfpCre* mice fed 0.5% cholic acid corrected by flow rate. Contributions of individual bile acids to the total bile acid pool are listed as percentages in parenthesis. Abbreviations: CA, cholic acid; C, cholanoate; T, tauro; G, glyco; DiOH, dihydroxy; tetraOH, tetrahydroxy.

Biliary concentrations (nmol/min.100g)							
Bile acid	*Vps33b*$^{fl/fl}$			*Vps33b*$^{fl/fl}$*-AlfpCre*			Comparison
	Median	25th Percentile	75th Percentile	Median	25th Percentile	75th Percentile	P value (Mann Whitney)
TCA	47.26 (68.48%)	33.76	53.74	90.42 (92.26%)	70.67	99.24	0.0667(ns)
GCA	2.93 (4.25%)	2.12	3.99	1.58 (1.61%)	0.98	2.88	0.2571 (ns)
CA	11.21 (16.24%)	7.28	11.60	0.84 (0.86%)	0.14	4.55	0.0190
Tauro-diOH-C	7.30 (10.58%)	4.96	8.41	4.93 (5.03%)	2.74	6.23	0.0667(ns)
Glyco-diOH-C	0.18 (0.26%)	0.15	0.21	0.21 (0.21%)	0.19	0.27	0.1714 (ns)
DiOH-C	0.13 (0.19%)	0.08	0.31	0.03 (0.03%)	0.00	0.08	0.1143(ns)

Figure Legends

Fig.1. ARC liver disease in *Vps33b*$^{fl/fl}$*-AlfpCre* mice. (**A**) Plasma ALP activity, (**B**) plasma ALT activity (**C**) liver mass and (**D**) total plasma bile acid levels assessed in 14-week-old normal chow fed and cholic acid (CA) fed *Vps33b*$^{fl/fl}$*-AlfpCre* and *Vps33b*$^{fl/fl}$ mice (n=4-6). (**E**) Trichrome staining of liver sections from 14-week-old CA fed mice and 12-month-old mice fed with normal diet (n=3). Graphs are presented with medians and IQR. P-values (Mann Whitney U test): ALP activity, P=0.0317 and P=0.0022; ALT activity P=0.0591 and P=0.1775; plasma bile acids, P=0.0043 and

P=0.0022; liver mass, P=0.0117 and P=0.0050 (normal chow fed and CA fed comparisons respectively).

Fig.2. Functional polarity defects in *Vps33b$^{fl/fl}$-AlfpCre* mice. (**A**) Immunostaining for detection of BSEP and (**B**) MRP2 localisation in *Vps33b$^{fl/fl}$-AlfpCre* and *Vps33b$^{fl/fl}$* liver sections. (**C**) Plasma and bile levels of cholesterol and (**D**) phospholipid in *Vps33b$^{fl/fl}$-AlfpCre* and *Vps33b$^{fl/fl}$* mice assessed by fluorometric analysis (n=5, P=0.0079 in all tests, Mann Whitney U test). (**E**) Cumulative biliary levels of CLF and (**F**) blood levels of CLF measured in *Vps33b$^{fl/fl}$-AlfpCre* and *Vps33b$^{fl/fl}$* (n=4). All mice were fed a cholic acid supplemented diet and sacrificed at 14-15 weeks of age. Graphs are presented with medians and IQR.

Fig.3. Gene expression analysis. Heat map showing gene expression of the top 50 genes identified as differentially expressed by PLS loading in the first component. Analysis was performed on liver RNA samples from 10-14-week-old, cholic acid fed *Vps33b$^{fl/fl}$* and *Vps33b$^{fl/fl}$-AlfpCre* mice. Color Key: 4 (red) =lower expression level; 12 (yellow) =higher expression level. Left hand trees link genes with similar expression patterns but do not necessarily infer a functional relationship.

Fig.4. *In vivo* gene transfer of human *VPS33B*. (**A**) Schematic of ssAAV2/8 vectors containing wild type (*hVPS33B*) and codon optimised (*hVPS33Bco*) human *VPS33B* cDNA. (**B**) Plasma alkaline phosphatase activity levels (P=0.0016, Kruskal-Wallis test), (**C**) total plasma bile acid levels (P=0.0015, Kruskal-Wallis test) (**D**) Plasma cholesterol levels (P=0.0023, Kruskal-Wallis test) (**E**) plasma phospholipid levels (P=0.0047, Kruskal-Wallis test) and (**F**) CEA protein localisation assessed 9 weeks after injection of ssAAV2/8-EFS-*hVPS33B*-WPRE and ssAAV2/8-EFS-*hVPS33Bco*-WPRE (1×10^{12}vg/mouse) in 5 week old *Vps33b$^{fl/fl}$-ALFPCre* mice (n=4-

6). All mice were fed cholic acid supplemented diet and sacrificed at 14 weeks of age. Graphs are presented with medians and IQR.

Fig.5. Tight junction defects in *Vps33b$^{fl/fl}$-AlfpCre* mice. Appearance of hepatocellular tight junctions assessed by immunostaining for Claudin1 in (**A**) *Vps33b$^{fl/fl}$* and (**B**) *Vps33b$^{fl/fl}$-AlfpCre* mouse liver sections and in (**C**) sections of *Vps33b$^{fl/fl}$-AlfpCre* mouse liver 9 weeks after injection of ssAAV2/8-EFS-*hVPS33Bco*-WPRE vector (1×10^{12}vg/mouse injected at 5 weeks of age) (n=3). (**D**) Cumulative FD-40 levels measured in bile fractions from *Vps33b$^{fl/fl}$-AlfpCre* and *Vps33b$^{fl/fl}$* mice collected after intravenous FD-40 injection (n=4-5, P=0.0134). All mice were fed a cholic acid supplemented diet and sacrificed at 14-15 weeks of age.

Fig.6. Bile canaliculus ultrastructure. Transmission electron micrographs of bile canaliculi in (**A**) *Vps33b$^{fl/fl}$* and (**B**) *Vps33b$^{fl/fl}$-AlfpCre* mouse liver and in (**C**) liver of *Vps33b$^{fl/fl}$-AlfpCre* mice injected with 1×10^{12}vg/mouse of ssAAV2/8-EFS-*hVPS33Bco*-WPRE vector. (**D**) Measurements of canalicular membrane length (±SEM) as a factor of canalicular perimeter assessed using ITEM software on mouse hepatocyte electron micrographs (n=62-90, P=<0.0001, One way ANOVA, Bonferroni's test). All mice were fed a normal chow diet and sacrificed at 14-15 weeks of age.

Figure 1

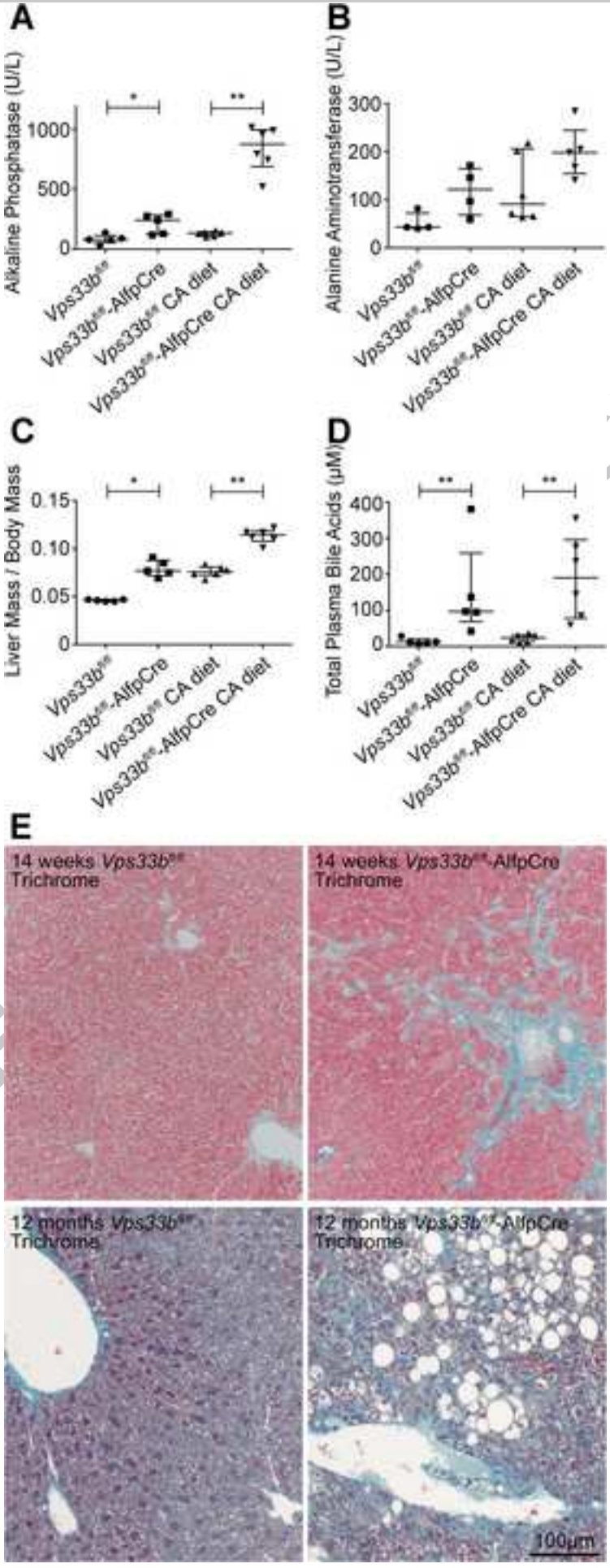

Figure 2

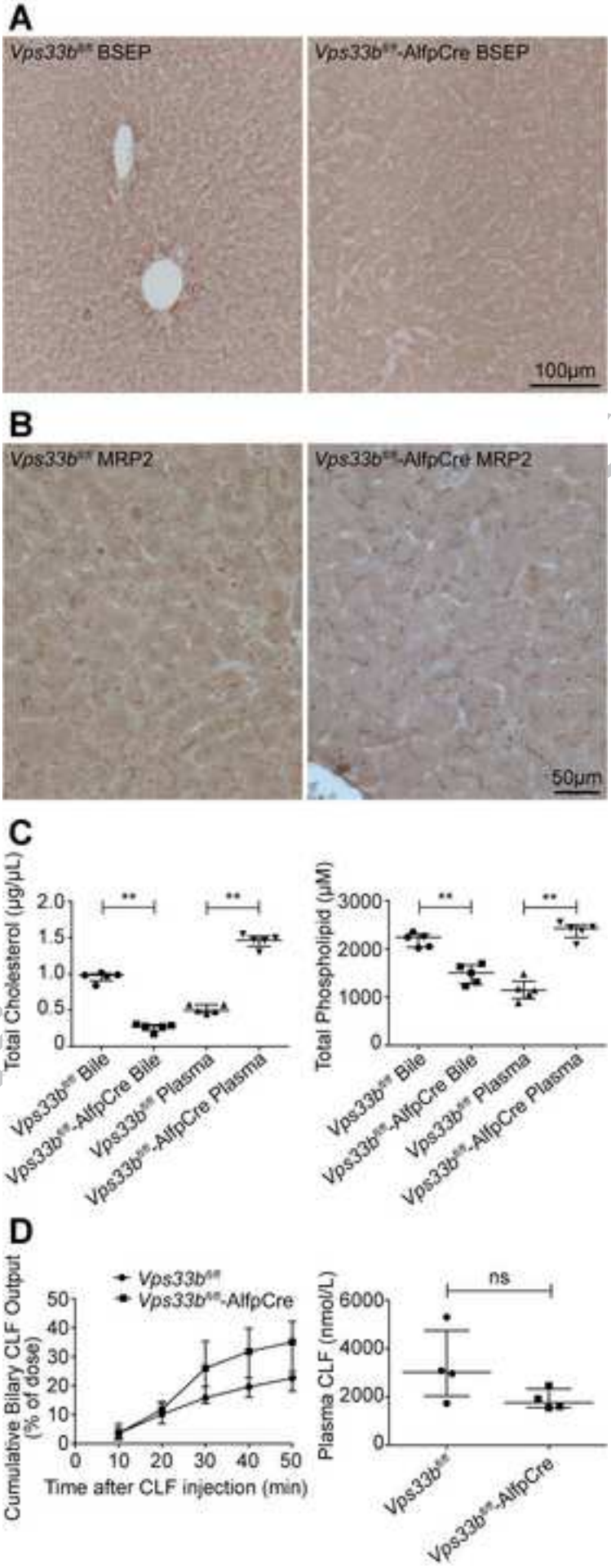

Figure 3

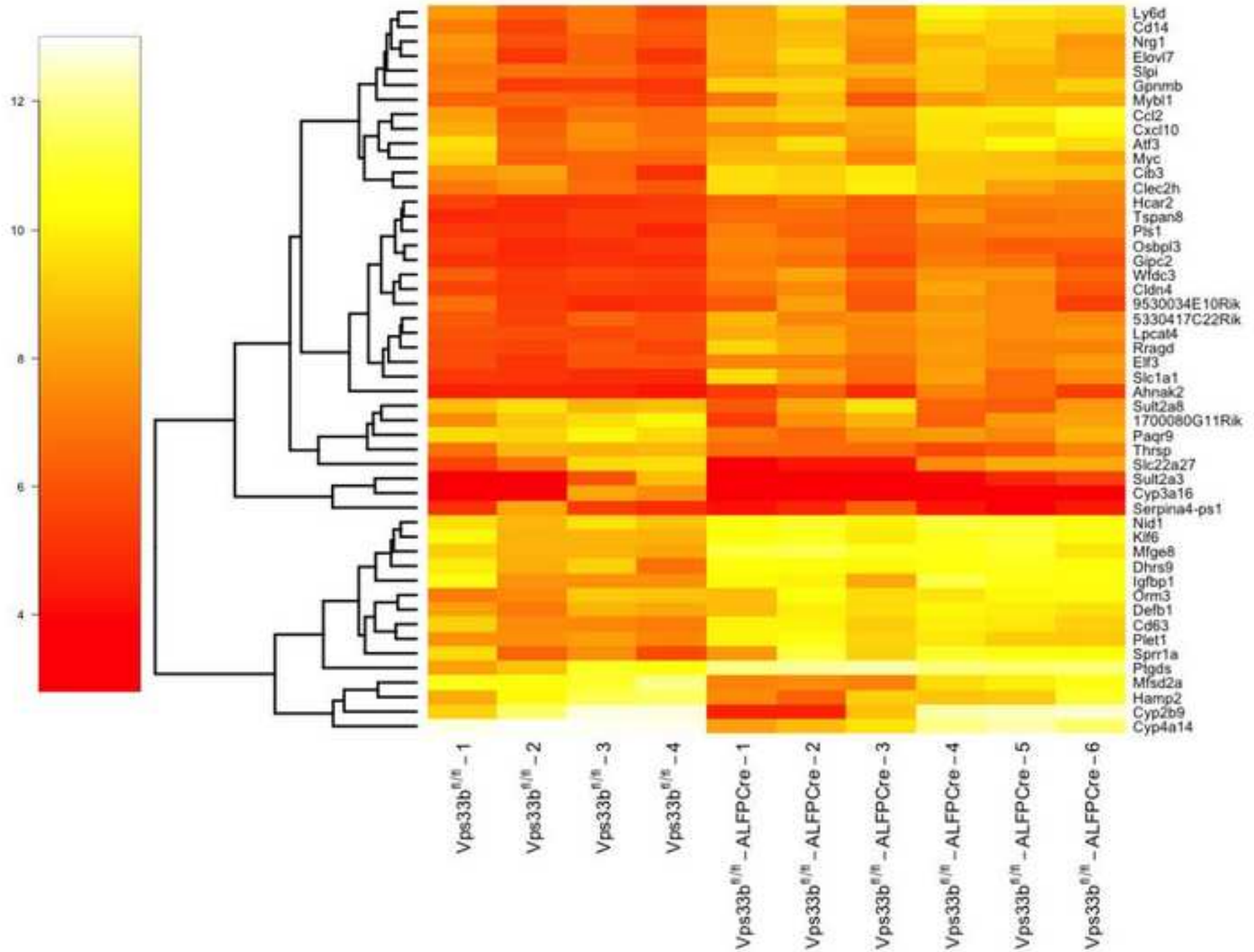

Figure 4

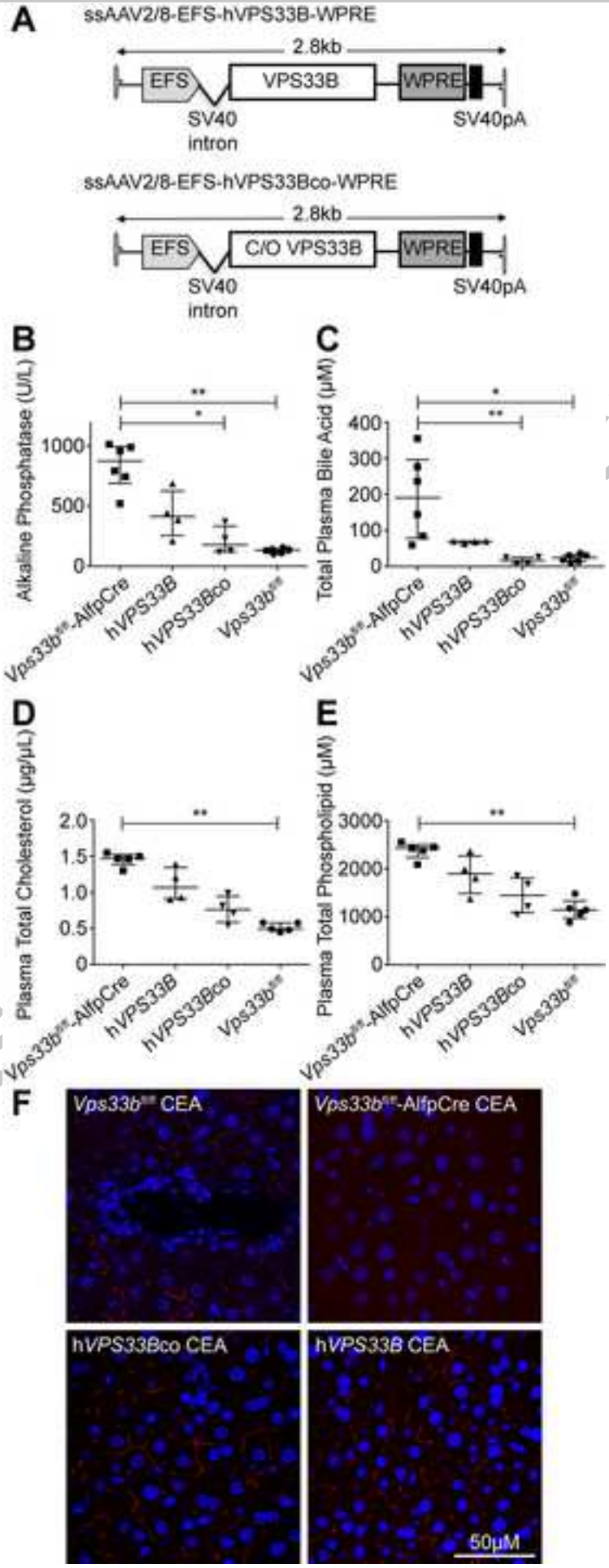

Figure 5

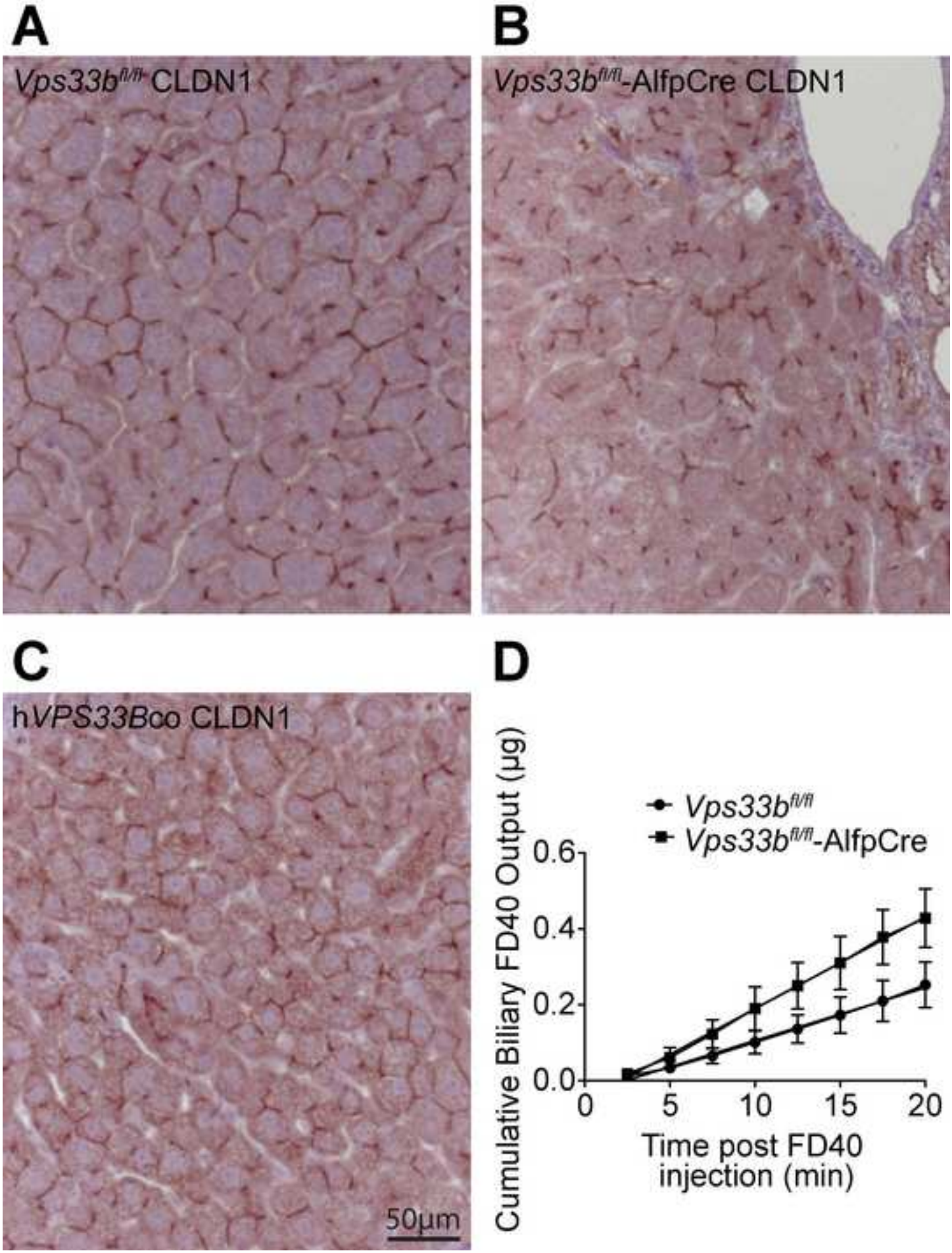

Figure 6

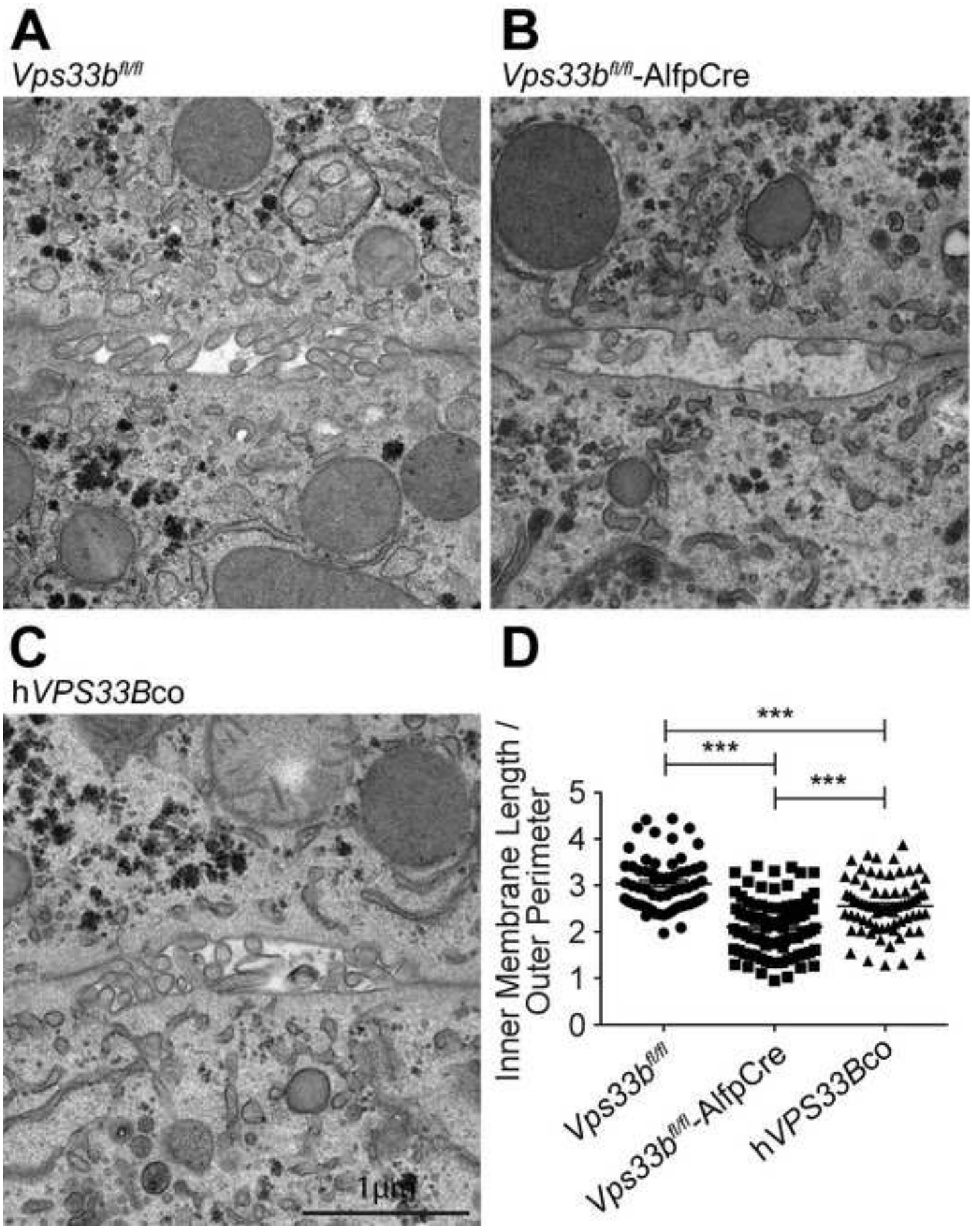

Graphical Abstract